Accepted Manuscript

Graphene oxide directed *in-situ* deposition of electroactive silver nanoparticles and its electrochemical sensing application for DNA analysis

Ningning Gao, Feng Gao, PhD., Suyu He, Qionghua Zhu, Jiafu Huang, Hidekazu Tanaka, Prof. Qingxiang Wang

PII: S0003-2670(16)31375-7

DOI: 10.1016/j.aca.2016.11.033

Reference: ACA 234904

To appear in: *Analytica Chimica Acta*

Received Date: 14 October 2016

Revised Date: 16 November 2016

Accepted Date: 21 November 2016

Please cite this article as: N. Gao, F. Gao, S. He, Q. Zhu, J. Huang, H. Tanaka, Q. Wang, Graphene oxide directed *in-situ* deposition of electroactive silver nanoparticles and its electrochemical sensing application for DNA analysis, *Analytica Chimica Acta* (2016), doi: 10.1016/j.aca.2016.11.033.

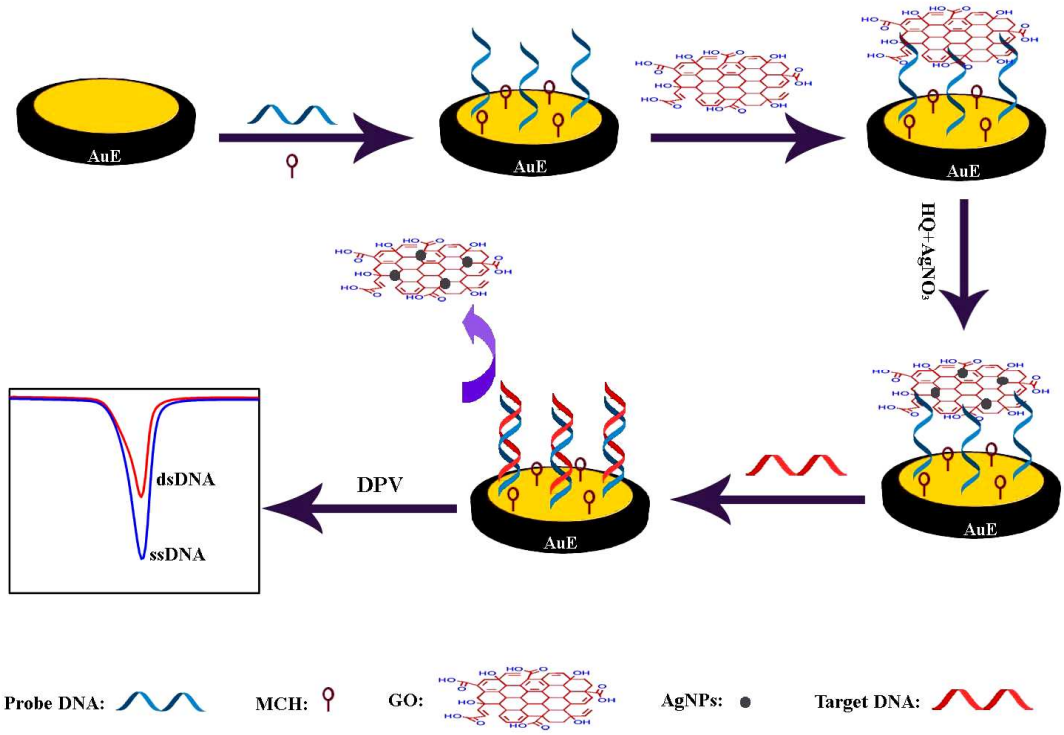

ACA16-2348Rev

Graphene oxide directed *in-situ* deposition of electroactive silver nanoparticles and its electrochemical sensing application for DNA analysis

Ningning Gao[a], Feng Gao[a,b,*], Suyu He[a], Qionghua Zhu[a], Jiafu Huang[a], Hidekazu Tanaka[b], Qingxiang Wang[a,*]

[a] *College of Chemistry and Environment, Fujian Province Key Laboratory of Modern Analytical Science and Separation Technology, Minnan Normal University, Zhangzhou 363000, P. R. China*

[b] *Department of Chemistry, Graduate School of Science and Engineering, Shimane University, 1060 Nishikawatsu, Matsue, Shimane 690-8504, Japan*

**Authors for correspondence*

PhD. Feng Gao

Tel: +86-596-2591445;

Fax: +86-596-2520035.

E-mail: fgao1981@mnnu.edu.cn

***Prof.* Qingxiang Wang**

Tel: +86-596-2591445;

Fax: +86-596-2520035.

E-mail: axiang236@126.com

Submitted to: ***Analytica Chimica Acta***

Abstract: The development of high-performance biosensing platform is heavily dependent on the recognition property of the sensing layer and the output intensity of the signal probe. Herein, we present a simple and highly sensitive biosensing interface for DNA detection on the basis of graphene oxide nanosheets (GONs) directed *in-situ* deposition of silver nanoparticles (AgNPs). The fabrication process and electrochemical properties of the biosensing interface were probed by electrochemical techniques and scanning electron microscopy. The results indicate that GONs can specifically adsorb at the single-stranded DNA probe surface, and induces the deposition of highly electroactive AgNPs. Upon hybridization with complementary oligonucleotides to generate the duplex DNA on the electrode surface, the GONs with the deposited AgNPs will be liberated from the sensing interface due to the inferior affinity of GONs and duplex DNA, resulting in the reduction of the electrochemical signal. Such a strategy combines the superior recognition of GONs toward single-stranded DNA and double-stranded DNA, and the strong electrochemical response of *in-situ* deposited AgNPs. Under optimal conditions, the biosensor can detect target DNA over a wide range from 10 fM to 10 nM with a detection limit of 7.6 fM. Also, the developed biosensor shows outstanding discriminating ability toward oligonucleotides with different mismatching degrees.

Keywords:

Electrochemical sensor,

Graphene oxide nanosheets,

Silver nanoparticles,

In-situ deposition,

DNA Hybridization.

1. Introduction

High-performance DNA analysis through rapid and simple strategy has attracted extensive attention over the past decade in lots of areas, such as molecular test system [1], environmental regulation [2], disease diagnosis [3], and forensic human identification [4]. Up to date, diverse strategies have been exploited for DNA analysis, which includes surface-enhanced Raman scattering [5], quartz crystal microbalance [6], luminescent spectroscopy [7], polymerase chain reaction [8], and electrochemistry [9,10]. Of them, the electrochemistry-based sensing approaches receive widespread concerns due to their merits of simple operation process, fast signal output, low cost, and easy to miniaturization. Nowadays, in order to meet the higher requirement of DNA analysis in different fields, the electrochemical DNA biosensors have been coupled with other technologies to enhance their analytical ability. For example, numerous nanostructured materials have been employed to construct the novel sensing platforms to improve the recognition property of the sensing layer and the signal output intensity of the sensing event [11, 12].

Silver, as an important precious metal, has attracted considerable research interest for its distinct physicochemical properties and relatively low toxicity [13]. In recent years, silver nanoparticles (AgNPs) that combine the features of both silver and nanomaterials, show exponential increasing production in various fields. For example, based on their size and shape-depending optical, electrical, and magnetic properties, the application of AgNPs can be extended to antibacterial agents, sensor fabrication, composite fibers, cosmetics, and electronic components [14]. In the electrochemical field, AgNPs also show great potential since they have excellent electrocatalytic property toward many molecules such as H_2O_2 [15], gallic acid [16], azathioprine [17] and nitroaromatic compounds [18]. In addition, AgNPs have also been utilized as electrochemical tags for the biosensing analysis owing to their excellent electronic conductivity and electroactivity. Li et al. [19] have developed an approach for multiplexed DNA electrochemical detection based on oligonucleotide-functionalized AgNP tags aggregation. The result showed that the biosensor presented an ultralow detection limit of 5 aM for Hepatitis B virus (HBV) DNA fragments, contributing from the excellent electroactive property of the AgNPs aggregates. Similarly, another signal-amplified electrochemical aptamer sensing strategy based on

hybridization-inducing aggregates of DNA-AgNPs has been designed by Song et al. [20], through which multi-analytes determination with good analytical performance in clinical diagnostics was obtained. More recently, Yang et al. [21] have constructed a label-free electrochemical biosensor for miRNA-199a detection via direct synthesis of AgNPs on cytosine (C)-rich loop-structured oligonucleotides. All these studies demonstrate that AgNPs own great potential in the electrochemical biosensing analysis.

Graphene oxide nanosheets (GONs), as a novel carbon material, have received considerable interests from both the theoretical and the experimental scientists in the past decade [22]. Their excellent water-solubility, rich functional groups, large surface-to-volume ratio, easy preparation route, and outstanding fluorescence property offer them widespread applications in biomolecule sensing [23], protein assay [24], drug delivery and release [25], and living cells probing [26]. It has also been reported that the GONs can specifically interact with oligonucleotides through the unique π-stacking interaction [27]. However, when the oligonucleotides were hybridized with complementary sequences to form the double-helix structure, the interaction between the GONs and DNA will be greatly inhibited. Based on this fact, many electrochemical and spectroscopic GONs-based DNA biosensors have been developed [28-31]. In addition, the AgNPs-GONs composite has also attracted numerous attentions by researchers [32-34]. This, on one hand, is because the composites combine the properties of both AgNPs and GONs, and on the other hand, the stability and loading amount of AgNPs can be significantly enhanced by GONs due to the unique interaction between the two species [33]. More importantly, it is recently reported that the GONs can effectively catalyze the deposition of AgNPs due to the intrinsic reduction characteristic and rich active groups of GONs [34].

Inspired by these fantastic discoveries mentioned above, a new electrochemical DNA sensing strategy was established using GONs as a nano-scale functional supporting platform to direct and catalyze the *in-situ* deposition of AgNPs for the first time. First, the thiolated specific probe DNA was assembled on the surface of a gold electrode (AuE), and then the prepared GONs were attached on the electrode surface by unique π-stacking interaction with the DNA probe. Followed by, the electrode was immersed into Ag(I)/hydroquinone (HQ) mixture solution, from which the AgNPs was directly deposited

on the surface of GONs. Then when the probe DNA is hybridized with target sequences, the pre-adsorbed GONs with the deposited AgNPs will liberate from the biosensor surface, due to the strong interaction of GONs with free single-stranded DNA rather than duplex DNA. As a result, the electrochemical signal from the AgNPs on the biosensor is decreased, achieving the purpose for the target DNA monitoring and analysis. As a whole, this strategy ingeniously combines multiple characteristics of GONs such as unique binding selectivity with single-stranded DNA, special catalyzing activity toward the reduction of Ag(I) to electroactive AgNPs, and its nanosized effect for signal enhancement, to improve the analytical performance of the biosensor. The protocol also presents great potentials in the construction of highly sensitive and selective aptasensors and immunosensors.

2. Experimental

2.1 Reagents

GONs were synthesized according to the method reported by Hummers with minor modification using graphite as the raw material [35]. Hydroquinone (HQ) and silver nitrate ($AgNO_3$) were purchased from Guangdong Xilong Chemical Co. Ltd. (China). Tris (2-chloroethyl) phosphate (TCEP) was supplied by Sigma-Aldrich Reagent Co. Ltd. (China). 6-Mercapto-1-Hexanol (MCH) was provided by Beijing Ansimosen Technology Co. Ltd. (China). All the other chemical reagents used in this work were of analytical grade and obtained commercially. All the solutions throughout the experiments were prepared with doubly distilled water.

The 18-mer probe sequence (S1, 5'-SH-TCTTTGGGACCACTGTCG-3') from cauliflower mosaic virus 35S (CaMV 35S) promoter gene, complementary target sequence (S2, 5'-CGACAGTGGTCCCAA AGA-3'), one-base-mismatch sequence (S3, 5'-CGACAGTGGTCCCAACGA-3'), three-base-mismatch sequence (S4, 5'-CGACAATGGCCCCAACGA-3') and non-complementary sequence (S5, 5'-GCATCCAGCGAGCACGTA-3') were synthesized by Shanghai Sangon Bio-engineering Co. Ltd. (China). The probe DNA (S1) solution was prepared with immobilization buffer (pH 7.4) consisting of 20 mM Tris-HCl, 100 mM NaCl, 5 mM $MgCl_2$ and 10 mM TCEP. The other DNA sequences solutions were prepared with TE

(Tris-EDTA, pH 8.0).

2.2 Instrumentals

The morphologic variation of the electrode during step-by-step assembly of GONs and AgNPs were examined by JEOL JSM-6010LA scanning electron microscopy with an accelerating voltage of 10 kV (Japan). Electrochemical tests such as cyclic voltammetry (CV), electrochemical impedance spectroscopy (EIS) and differential pulse voltammetry (DPV) applied in this work were recorded on a CHI 650C electrochemical workstation (China), with a conventional three-electrode system consisting a modified AuE (Φ=3 mm) as working electrode, an Ag/AgCl (3M KCl) as reference electrode, and a platinum wire as counter electrode.

2.3 Preparation of the AgNPs/GNOs-based biosensor

Fig. 1 depicts the fabrication and hybridization detection process of the AgNPs/GONs-based biosensor. The detailed procedures are as follows: first, a bare AuE was carefully polished with 1.0 μm, 0.3 μm and 0.05 μm α-Al_2O_3, in turn on polishing clothes, and then successively washed with water, absolute ethanol and water in ultrasonication bath. After that, the polished AuE was chemically cleaned in Piranha solution (V(98%H_2SO_4):V(30% H_2O_2)=7:3) for 20 min to remove the organic pollutants adsorbed on the electrode surface. Furthermore, AuE was electropolished via cyclic voltammetry in 0.5 M H_2SO_4 within the potential range from -0.2 to +1.5 V until reproducible voltammetric curves were obtained.

After further washed with water, the AuE was incubated in 0.1 μM probe DNA (S1) solution at 4 □ for 24 h to form S1 modified electrode (S1/AuE). Followed by rinsing with TE and water for three times, the S1/AuE was transferred to an ethanol solution containing 1.0 mM MCH and reacted for 2 h to passivate the residue site of AuE surface. The obtained electrode was recorded as S1-MCH/AuE. Through such a procedure, the non-specific adsorption of the analytes on the AuE can be effectively prevented, and meanwhile, the probe DNA immobilized on AuE will be erected up, facilitating to binding with target DNA. Followed by, the electrode was incubated in 10 mL 0.1 mg mL^{-1} GONs aqueous solution for 2.5 h to assemble GONs layer. After gentle rinsing with DDW, the electrode was immediately incubated in 10 mL 0.1 mg mL^{-1} $AgNO_3$ solution containing 2 mg mL^{-1} HQ

for 5 min to deposit the AgNPs. After further washing with DDW, the AgNPs assembled electrode (AgNPs/GONs/S1-MCH/AuE) was achieved.

Here is Fig. 1

2.4 Hybridization and electrochemical test

The hybridization capacity of the fabricated biosensor was investigated by incubating AgNPs/GONs/S1-MCH/AuE into a solution containing target DNA (S2) with desired concentrations for 40 min under 42 □ with gentle shaking. After rinsing with TE to remove the non-specifically attached DNA, the hybridized electrode was achieved. The procedure was also applied for the hybridization of the biosensor with the other noncomplementary and base-mismatched DNA fragments.

The electrochemical characterization on the fabrication of the biosensing layer was obtained through cyclic voltammetry (CV) and electrochemical impendence spectra (EIS) in the mixture solution of 1.0 mM $[Fe(CN)_6]^{3-/4-}$ (1:1) and 0.1 M KCl. The scan rate in CV was 0.1 V s^{-1} and the frequency range in EIS was from 0.01 Hz to 10^4 Hz at an applied potential of +0.200 V. The electrochemical response of the fabricated biosensor (AgNPs-GONs/S1-MCH/AuE) was measured by cyclic voltammetry and differential pulse voltammetry (DPV) in 0.1 M KCl. The potential range was between -0.2 V and +0.6 V.

3. Results and discussion

3.1 SEM characterization

The fabrication process of AgNPs-GONs/S1-MCH/AuE was first characterized by SEM, and the results are displayed in Fig. 2. As seen, a smooth surface was observed for S1-MCH/AuE (Fig. 2A), suggesting the bare AuE had been successfully polished and the S1-MCH layer could not be reflected by the SEM characterization due to the molecular level of S1-MCH mixture layer. When GONs were adsorbed on the surface of the electrode, one can clearly see that the electrode surface become coarse, and some wrinkles corresponding to the typical crumpled texture of GONs appeared (Fig. 2B), which indicates that GONs have been well assembled on S1-MCH/AuE. Then, after the GONs/S1-MCH/AuE was incubated in Ag(I) /HQ mixture solution for 5 min, it is observed that a mass of bright particles is uniformly distributed on the surface of

GONs/S1-MCH/AuE (Fig. 2C). From the high-resolution SEM of the electrode (Fig. 2D), the average diameter of the obtained particles was determined to be about 100 nm. The EDS result from the electrode surface further demonstrates that, besides the elements of Au, N, C from the matrix material of the GONs/S1-MCH/AuE, the element of Ag can be well detected (Fig. 2F). Therefore, it can be concluded that the AgNPs had been successfully grown on GONs/S1-MCH/AuE as expected. As a control, the SEM image of GONs/MCH-S1/AuE after incubation in HQ solution without Ag(I) was also recorded (Fig. 2E), and it is observed that in contrast to the case containing Ag(I), not any bright dot is visible. This further testifies that the bright particles appeared in Fig. 2C are the metallic silver that reduced from Ag(I).

Here is Fig. 2

3.2 Electrochemical characterization

Here is Fig. 3

The step-by-step fabrication process of AgNPs-GONs/S1-MCH/AuE was also probed by CV (Fig. 3A) and EIS (Fig. 3B) in $[Fe(CN)_6]^{3-/4-}$ solution. From Fig. 3A, it is clearly observed that a couple of well-defined Faradic redox peaks corresponding to the electron transfer of $[Fe(CN)_6]^{3-}/[Fe(CN)_6]^{4-}$ is observed on bare AuE with the peak-to-peak separation (ΔE_p) of 90 mV (curve a), suggesting that the bare GCE has been well cleaned. When the AuE was modified with probe DNA (S1) through Au-S bond, the redox peaks of $[Fe(CN)_6]^{3-/4-}$ couple decrease distinctly, and the ΔE_p increases to 135 mV (curve b), which suggests that the thiolated probe DNA has been anchored on AuE surface, and as a consequence, the electrochemical response of $[Fe(CN)_6]^{3-/4-}$ is inhibited by the electrostatic repulsion force from the negative phosphate backbone of the probe DNA. Upon further modification with MCH, the redox peaks of $[Fe(CN)_6]^{3-/4-}$ decrease further as curve c in Fig. 3A displays, suggesting the occupation of the residue sites on S1/AuE by the MCH molecules. After the S1-MCH/AuE was incubated in GONs solution, the redox peaks of $[Fe(CN)_6]^{3-/4-}$ decrease once again (curve d), which can be explained by the reason that GONs attach on S1-MCH/AuE through π-stacking with the probe DNA strands, and its

inferior conductivity and negatively charged oxygen-containing groups such as –COOH, –OH and epoxy group further block the electrochemical reaction of $[Fe(CN)_6]^{3-/4-}$ probe.

Electrochemical impendence spectroscopy (EIS) was also utilized to characterize the assembly of probe DNA, MCH and GONs on AuE. In EIS, a typical Nyquist plot commonly consists of a semicircle portion at high-frequency region relating to the electron transfer-controlled process and a linear portion at low-frequency region corresponding to the diffusion-controlled process. The value of surface electron transfer resistance (R_{ct}) can be simply measured from the semicircle diameter in the high-frequency region of the plot [36]. The typical Nyquist plots of AuE upon layer-by-layer assembly with different materials are displayed in Fig. 3B. Only a linear portion is observed on bare AuE, showing that the electrochemical response of $[Fe(CN)_6]^{3-/4-}$ on the bare AuE is mainly controlled by a diffusion process. After S1 and MCH were modified on AuE, large semicircles corresponding to the R_{ct} values of 1.6 kΩ (curve b) and 12.8 kΩ (curve c) are obtained, showing that the mixture layer of probe DNA and MCH have been successfully immobilized on AuE and block the approach of $[Fe(CN)_6]^{3-/4-}$ ions. When GONs were further assembled, the semicircle diameter increases again and the value of R_{ct} is increased to 18.0 kΩ (curve d), demonstrating that the negatively charged and non-conductive GONs have been assembled on S1-MCH/AuE.

3.3 Specific *in-situ* growth of electroactive AgNPs

Here is Fig. 4

It has been reported that Ag(I) can be chemically reduced by HQ to metallic silver, and the reduction process can be greatly catalyzed by the GONs [32, 34]. In this work, the GONs was used as a functional film to catalyze the *in-situ* deposition of AgNPs, for the construction of electroactive sensing interface. The electrochemical behavior of the obtained sensing film was investigated in KCl solution, and the results are showed in Fig. 4. From the CV result, one can see that there is not any Faradic signal on GONs/S1-MCH/AuE (curve a), suggesting that the probe electrode without deposited AgNPs is electro-inactive under the tested potential window. However, after the electrode

was incubated in the mixture solution of HQ and Ag(I), a pair of intense and sharp redox peaks appears at 0.13 V and -0.01 V (curve a), which is very close to the redox peak potential of metallic silver in the previous reports [37, 38]. This result also means that the electro-active AgNPs were successfully formed on the surface of GONs/S1-MCH/AuE. In addition, in order to investigate the effect of GONs on the formation of AgNPs, the S1-MCH/AuE without pre-adsorbed GONs was also incubated in the mixture solution of HQ and Ag^+, and then electrochemically detected under the same experimental conditions. The result (curve b) shows that only a couple of very tiny redox peaks appears, and the peak potentials negatively shifted as compared with those at GONs modified electrode. These results suggest that only little amount of AgNPs are formed on S1-MCH/AuE and the binding sites of AgNPs on the electrode might also be different when GONs are absent. This further confirms that GONs act as an effective functional platform to induce the large-scale growth of AgNPs at the electrode surface.

The cyclic voltammograms of AgNPs/GONs/MCH-S1/AuE at various scan rates (v) were also investigated. The results as depicted in Fig. 4B show that both the reduction and the oxidation peaks increase regularly with the increase of scan rate, and the peak currents present good linearity with the square root of scan rate ($v^{1/2}$) over the scan rate range from 10 to 500 mV s^{-1}: I_{pa} (10^{-5} A) = -15.2501 v(V/s)$^{1/2}$ +1.3953, r=0.9953 and I_{pc} (10^{-5} A) = 9.1134 v(V/s)$^{1/2}$ -0.5606, r=0.9974 (inset of Fig. 4B). This electrochemical characteristic demonstrates that the redox reaction of AgNPs is a diffusion-controlled process, which can be explained by the fact that the electrochemical reaction of AgNPs involves with the diffusion of Cl^- from the bulk solution to electrode surface via the following equation [39]:

$$\text{AgNPs/GONs/MCH-S1/AuE} + Cl^-(\text{solution}) = \text{AgCl/GONs/MCH-S1/AuE} + e^-$$

3.4 Feasibility of the biosensor for hybridization monitoring

Due to the unique honeycomb crystal structures, the GONs can specifically bind to single-stranded DNA through the π-stacking with the aromatic bases of oligonucleotides, whereas once the single-stranded DNA is hybridized with complementary sequences to form the duplex structure, the free bases of oligonucleotides will be buried within the duplex structure. As a consequence, the interaction between the GONs and single-stranded

DNA will be greatly inhibited [27, 28]. Based on this principle, the AgNPs/GONs/MCH-S1/AuE was utilized as an electrochemical biosensing platform using GONs/S1 as the recognition element and AgNPs as the signal-output source. Its feasibility for hybridization was investigated by monitoring electrochemical response variation of the electrode before and after incubation in the hybridization solution. Fig. 5A reveals the CVs of the biosensor before (curve a) and after (curve b) hybridization with 0.1 pM target DNA. The results clearly reveal that the electrochemical signal of AgNPs at the biosensor after hybridization decreases obviously, showing that the formation of the duplex DNA between S1 and S2 prohibits the interaction between GONs/AgNPs complex and single-stranded probe DNA, and thus the pre-adsorbed GONs with the deposited AgNPs is liberated from the biosensor surface, leading to the decrease of the electrochemical response. This also indicates that the GONs with the in-situ deposited AgNPs remain the feature of having the stronger affinity with single-stranded DNA than the rigid duplex DNA. So it can be deduced that the electroactive sensing interface of AgNPs/GONs/S1-MCH is feasible for hybridization monitoring.

In addition, the hybridization performance of the GONs-unadsorbed control electrode of S1-MCH/AuE with the directly deposited AgNPs was also investigated, and the result is displayed in Fig. 5B. It is found that the redox peaks in the cyclic voltammogram of AgNPs/S1-MCH/AuE decrease slightly after incubation in the hybridization solution. This suggests that the biosensing interface of S1/MCH/AuE with directly deposited AgNPs has inferior hybridization capacity in comparison with AgNPs/GONs/S1-MCH/AuE, which might be related to the fact that, when GONs is absent, the Ag(I) directly binds to DNA probe through electrostatic interaction with the phosphate backbone and coordination with bases, which changes the configuration of probe DNA and then impairs their hybridization ability. Therefore, it can be concluded that the developed biosensor based on adsorbed GONs with the deposited AgNPs has the good feasibility for hybridization monitoring as well as intense electrochemical response. Also, it is of note that the signal output is based on direct redox of the deposited AgNPs, which is much more convenient than the traditional metal sulfide tags-based biosensors that need fussy labeling of signal probe, harmful dissolution solution, and complicated adsorptive stripping voltammetric

measurement [40-42].

Here is Fig. 5

3.5 Optimization of experimental conditions

Fig. 6A shows the effect of immersing time (*t*) of S1/MCH/AuE in GONs solution on the R_{ct} values in EIS measurements. Clearly, with the prolonging the incubation time from 0 to 150 min, the R_{ct} values increased significantly, indicating that an increasing number of GONs were adsorbed on S1/MCH/AuE via interaction with S1. When the immersing time reaches 150 min, the R_{ct} values are hardly changed, which is an indication of the adsorption saturation of GONs. Therefore, 150 min was chosen for GONs adsorption. The AgNPs deposition experiment shows that when the GONs/S1/MCH/AuE was immersed into $AgNO_3$ and HQ mixture for 5 min, the electrochemical response of the biosensor researched the maximum value, which shows that 5 min is enough for the GONs-catalyzed deposition of AgNPs. Fig. 6B shows the relationship of the oxidation peak currents (I_{pa}) of the biosensor versus hybridization time (*t*). As shown, the oxidation peak currents decrease when hybridization time increase from 0 to 40 min and then level off, indicating that the hybridization reaction between S1 and S2 can finish within 40 min. Therefore, 40 min was selected as the optimal time for hybridization reaction in subsequent assays.

Here is Fig. 6

3.6 Analytical performance

The analytical performance of the biosensor was evaluated by investigating its sensitivity and selectivity. Fig. 7 shows the DPVs of AgNPs/GONs/MCH-S1/AuE upon hybridization with different concentrations of target DNA. It is found that the peak currents (I_{pa}) of AgNPs/GONs in DPV response decrease with increasing concentrations of target DNA (C_{S2}), which demonstrates that increasing amounts of duplex DNA are formed on the biosensor surface, and the bound amounts of AgNPs/GONs reduced accordingly. The values of I_{pa} of the biosensor presents a good correlation with the logarithmic values of C_{S2} ($\lg C_{S2}$) over the concentrations range from 10.0 fM to 10.0 nM (Fig. 7B) obeying a regression equation of $I_p/\mu A=0.6191 \log(C_{S2}/M)+8.161$, $r=0.9883$. The limit of detection (LOD) was then estimated to be 7.6 fM on the rule of 3 times the standard deviation over

the background signal. The linear range and LOD of the AgNPs/GONs/MCH-S1/AuE are also compared with the other AgNPs or graphene-based DNA electrochemical biosensors (Table 1). Clearly, the DNA biosensor presented in this work demonstrates the lowest LOD and the widest linear range. Such a high analytical performance can be ascribed to the excellent electroactivity of AgNPs and the high hybridization efficiency of GONs-mediated biosensing interface.

Here is Fig. 7

Here is Table 1

The selectivity is another important performance of a DNA biosensor. The high selectivity of a DNA biosensor to recognize the base-mismatching of analyzed DNA has the potential application in lots of fields such as species identification, gene-related diseases (tumors and cancers) diagnosis, and virus monitoring. In this work, the hybridization selectivity of AgNPs/GONs/MCH-S1/AuE was assessed through hybridization with different oligonucleotides. Fig. 8A is the DPVs of different hybridized electrodes and Fig. 8B is the corresponding histogram. As seen, the non-complementary sequence (S5) hybridized electrode (curve b) shows close DPV and peak current to the AgNPs/GONs/S1-MCH/AuE (curve a), which indicates that the hybridization reaction does not happen between probe DNA and the non-complementary DNA due to the complete base mismatch of the two sequences. However, when the AgNPs/GONs/S1-MCH/AuE was reacted with the CaMV 35S-related target sequence of S2, the oxidation peak signal in DPV decreases dramatically (curve e), confirming that the formation of double-helix DNA on the electrode, and the AgNPs/GONs composite was fallen off from the sensor surface by the hybridization process. The discriminating ability of the biosensor was also probed by hybridization with S3 with the one-mismatched base and S4 with three-mismatched bases. It is obtained that the values of oxidation peaks of AgNPs/GONs on the two hybridized electrodes are fall in the values between the probe electrode and the target DNA-hybridized electrode, which can be explained by reason that only partial base-pairing has happened for S3 and S4. Meanwhile, the value of oxidation peak current on AgNPs/GO/S4-S1-MCH/AuE (c) is higher than that on AgNPs/GO/S3-S1-MCH/AuE (d), suggesting that the AgNPs/GONs-based biosensor can also well recognize the DNA

fragments containing various mismatching number of base. All these results show that the developed DNA biosensor has significant potential application to monitor whether an organism is genetically modified or non-genetically modified.

Here is Fig. 8

3.7 Reproducibility, regeneration, and reliability

The reproducibility of the developed DNA sensing strategy was investigated by detecting 0.1 pM target sequences with five parallel-made electrodes of AgNPs/GONs/S1-MCH/AuE. The results show that a relative standard deviation (RSD) of 8.3% for the signal changes (ΔI_{pa}) was estimated, showing that the sensing strategy has an acceptable reproducibility for DNA detection. The regeneration of the biosensor was performed by immersing the hybridized electrode into the water at 90 □ for 6 min, and then cooled in an ice-water bath for 6 min to denature the hybridized duplex DNA. Afterward, the electrode was assumed with GONs and AgNPs again, for hybridization in the next round. The results show that the biosensor can be successively used for at least five rounds of assembly-hybridization-denaturation without losing its hybridization capacity. The reliability of the developed DNA biosensor was evaluated by a recovery experiment carried out in real serum samples. As shown in Table 2, when 0.1 nM, 1.0 pM and 10 fM target DNA sequences were respectively added into 50-times diluted serum samples, and measured five times for each sample, the recoveries and RSD were in the range of 95.2-107.0% and 3.98-5.67%, respectively. These results indicate that the developed sensing method has good precision and reliability for DNA analysis in real samples.

Here is Table 2

Conclusions

In summary, a novel nanostructured electrochemical DNA sensing platform was designed and constructed based on the use of GONs with in-situ deposited AgNPs as the sensing signal. The GONs were assembled on the probe DNA-modified electrode via the π-stacking force, which also acts as a catalyst for the direct deposition of electroactive AgNPs. Due to the excellent electrochemical activity of in-situ formed AgNPs, and differential interaction of GONs with signal-stranded and double-stranded DNA, the

constructed biosensor presents outstanding hybridization selectivity and sensitivity. The low detection limit of 5.2 fM was estimated, which can be ascribed to the excellent electroactivity of AgNPs and nano effect of GONs. Recovery experiment further means that the biosensor has good reliability. Such a GONs-AgNPs-based sensing interface presented in this work also represents a universal platform to be extended to immunosensors and aptasensors.

Acknowledgments

The work is supported by the National Natural Science Foundation of China (No. 21275127), Education-Science Research Project for Young and Middle-aged Teachers of Fujian (No. JA15305), and Scientific Fujian Province Universities Learning and Production Science and Technology Cooperative Major Projects (2012N5013).

References

[1] G.L. Xu, R.N. Gunson, J.M. Cooper, J.L. Reboud, Rapid ultrasonic isothermal amplification of DNA with multiplexed melting analysis-applications in the clinical diagnosis of sexually transmitted diseases, Chem. Commun. 51 (2015) 2589–2592.

[2] T. Takahara, T. Minamoto, H. Doi, Effects of sample processing on the detection rate of environmental DNA from the common carp (Cyprinus carpio), Biol. Conserv. 183 (2015) 64–69.

[3] E. Sanchez, W. Peng, C. Toro, C. Sanin, M. Graña, E. Szczerbicki, E. Carrasco, F. Guijarro, L. Brualla, Decisional DNA for modeling and reuse of experiential clinical assessments in breast cancer diagnosis and treatment, Neurocomputing 146 (2014) 308-318.

[4] P. Liu, X.J. Li, S.A. Greenspoon, J.R. Scherer, R.A. Mathies, Integrated DNA purification PCR, sample cleanup, and capillary electrophoresis microchip for forensic human identification, Lab Chip 11 (2011) 1041–1048.

[5] S.J. He, K.K. Liu, S. Su, J. Yan, X.H. Mao, D.F. Wang, Y. He, L.J. Li, S.P. Song, C.H. Fan, Graphene-based high-efficiency surface-enhanced Raman scattering-active platform for sensitive and multiplex DNA detection, Anal. Chem. 84 (2012) 4622–4627.

[6] Y Zhao, H.M. Wang, W. Tang, S.C. Hu, N. Lia, F. Liu, An in situ assembly of a DNA–streptavidin dendrimer nanostructure: a new amplified quartz crystal microbalance

platform for nucleic acid sensing, Show Affiliations Chem. Commun. 51 (2015) 10660-10663.

[7] J.D. Sun, J. Ji, Y.Q. Sun, M. H. Abdalhai, Y.Z. Zhang, X.L. Sun, DNA biosensor-based on fluorescence detection of E. coli O157:H7 by Au@Ag nanorods, Biosens. Bioelectron. 70 (2015) 239-245.

[8] W.P. Gan, B. Zhuang, P.F. Zhang, J.P. Han, C.X. Li, P. Liu, A filter paper-based microdevice for low-cost, rapid, and automated DNA extraction and amplification from diverse sample types, Lab Chip 14 (2014) 3719-3728.

[9] X.Y. Dong, X.N. Mi, L. Zhang, T.M. Liang, J.J. Xu, H.Y. Chen, DNAzyme-functionalized Pt nanoparticles/carbon nanotubes for amplified sandwich electrochemical DNA analysis, Biosens. Bioelectron. 38 (2012) 337–341.

[10] Q.X. Wang, F. Gao, J.C. Ni, X.L. Liao, X. Zhang, Z.Y. Lin, Facile construction of a highly sensitive DNA biosensor by in-situ assembly of electro-active tags on hairpin-structured probe fragment, Scientific Reports, 6 (2016) 22441.

[11] W.T. Shi, Z.F. Ma, Amperometric glucose biosensor based on a triangular silver nanoprisms/chitosan composite film as immobilization matrix, Biosens. Bioelectron. 26 (2010) 1098–1103.

[12] S. Lee, S. Shin, S.G. Lee, J. Seo, J.H. Lee, S.B. Son, H.J Cho., H. Algadi, S. Al-Sayari, D.E. Kim, T. Lee, Ag nanowire reinforced highly stretchable conductive fibers for wearable electronics, Adv. Funct. Mater. 25 (2015) 3114–3121.

[13] F.W. Campbell, S.R. Belding, R. Baron, L. Xiao, R.G. Compton, Hydrogen peroxide electroreduction at a silver-nanoparticle array: investigating nanoparticle size and coverage effects**,** J. Phys. Chem. C 113 (2009) 9053–9062.

[14] A. Shukla, B.A. Makwana, Facile synthesis of silver nanoparticle and their potential application, J.Nanosci. Nanotechno. 2 (2014) 84–92.

[15] P. Miao, B. Wang, J. Yin, X. Chen, Y. Tang, Electrochemical tracking hydrogen peroxide secretion in live cells based on autocatalytic oxidation reaction of silver nanoparticles, Electrochem. Commun. 53 (2015) 37–40.

[16] M. Ghaani, Development of an electrochemical nanosensor for the determination of gallic acid in food, Anal. Methods 8 (2016) 1103–1110.

[17] E. Asadian, A.I. Zad, S. Shahrokhian, Voltammetric studies of azathioprine on the surface of graphite electrode modified with graphene nanosheets decorated with Ag nanoparticles, Mater. Sci. Eng. C 58 (2016) 1098–1104.

[18] X. Chen, X.Y. Cheng, G.J. Justin, Detection of trace nitroaromatic isomers using indium tin oxide electrodes modified using β-cyclodextrin and silver nanoparticles, Anal. Chem. 84 (2012) 8557−8563.

[19] H. Li, Z. Sun, W. Zhong, N. Hao, D. Xu, H.Y. Chen, Ultrasensitive electrochemical detection for DNA arrays based on silver nanoparticle aggregates. Anal. Chem. 82 (2010) 5477–5483.

[20] W. Song, H. Li, H. Liang, W.B. Qiang, D.K. Xu, Disposable electrochemical aptasensor array by using in situ DNA hybridization inducing silver nanoparticles aggregate for signal amplification, Anal. Chem. 86 (2014) 2775–2783.

[21] C.Y. Yang, K. Shi, B.T. Dou, Y. Xiang, Y.Q. Chai, R. Yuan, In situ DNA-templated synthesis of silver nanoclusters for ultrasensitive and label-free electrochemical detection of micro-RNA, ACS Appl. Mater. Interfaces 7 (2015) 1188−1193.

[22] S. Mao, H.H. Pu, J.H. Chen, Graphene oxide and its reduction: modeling and experimental progress, RSC Adv. 2 (2012) 2643–2662.

[23] Y. Wang, Z.H. Li, T.J. Weber, D.H. Hu, C.T. Lin, J.H. Li, Y.Y. Lin, In situ live cell sensing of multiple nucleotides exploiting DNA/RNA aptamers and graphene oxide nanosheets, Anal. Chem. 85 (2013) 6775–6782.

[24] X.W. Chen, X. Hai, J.H. Wang, Graphene/graphene oxide and their derivatives in the separation/isolation and preconcentration of protein species: A review. Anal. Chim. Acta 922 (2016) 1–10.

[25] P. Gao, M.Y. Liu, J.W. Tian, F.J. Deng, K. Wang, D.Z. Xu, L.J. Liu, X.Y. Zhang, Y. Wei, Improving the drug delivery characteristics of graphene oxide based polymer nanocomposites through the “one-pot” synthetic approach of single-electron-transfer living radical polymerization, Appl. Surf. Sci. 378 (2016) 22–29.

[26] S. Sreejith, X. Ma, Y.L. Zhao, Graphene oxide wrapping on squaraine-loaded mesoporous silica nanoparticles for bioimaging, J. Am. Chem. Soc. 134 (2012) 17346–17349.

[27] B.W. Liu, Z.Y. Sun, X. Zhang, J.W. Liu, Mechanisms of DNA sensing on graphene oxide, Anal. Chem. 85 (2013) 7987–7993.

[28] A. Bonanni, C.K. Chua, G.J. Zhao, Z. Sofer, M. Pumera, Inherently electroactive graphene oxide nanoplatelets as labels for single nucleotide polymorphism detection, ACS Nano 6 (2012) 8546–8551.

[29] A. Wu, Q. Wang, Q. Zhu, J. Ni, F. Gao, A facile and highly sensitive impedimetric DNA biosensor with ultralow background response based on in-situ reduced graphene oxide, RSC Adv. 5 (2015) 90983–90990.

[30] B. Eftekhari-Sis, M.A. Aliabad, F. Karimi, Graphene oxide based nano-biosensor for the detection of deletion mutation in exon 19 of EGFR gene, leading to lung cancer, Mater. Lett. 183 (2016) 441–443.

[31] X.Q. Liu, R. Aizen, R. Freeman, O. Yehezkeli, I. Willner, Multiplexed aptasensors and amplified DNA sensors using functionalized graphene oxide: Application for logic gate operations, ACS Nano 6 (2012) 3553–3563.

[32] M. Veerapandian, Y.T. Seo, K. Yun, M.H. Lee, Graphene oxide functionalized with silver@silica–polyethylene glycol hybrid nanoparticles for direct electrochemical detection of quercetin, Biosens. Bioelectron. 58 (2014) 200–204.

[33] H.W. Bai, L. Liu, D.D. Sun, Stability investigation of graphene oxide–silver nanoparticles composites in natural reservoir water, RSC Adv. 3 (2013) 25331–25339.

[34] Y. Wan, Y. Wang, J.J. Wu, D. Zhang, Graphene oxide sheet-mediated silver enhancement for application to electrochemical biosensors, Anal. Chem. 83 (2011) 648–653.

[35] W. Hummers, R. Offeman, Preparation of graphitic oxide, J. Am. Chem. Soc. 80 (1958) 1339–1339.

[36] F. Gao, X.L. Cai, X. Wang, C. Gao, S.L. Liu, F. Gao, Q.X. Wang, Highly sensitive and selective detection of dopamine in the presence of ascorbic acid at graphene oxide modified electrode, Sens. Actuators B: Chem 186 (2013) 380–387.

[37] E. Prabakaran, K. Pandian, Amperometric detection of Sudan-I in red chili powder samples using Ag nanoparticles decorated graphene oxide modified glassy carbon electrode, Food Chem. 166 (2015) 198–205.

[38] H. Zhu, M.L. Du, M. Zhang, P. Wang, S.Y. Bao, L.N. Wang, Y.Q. Fu, J.M. Yao, Facile fabrication of AgNPs/(PVA/PEI) nanofibers: high electrochemical efficiency and durability for biosensors, Biosens. Bioelectron. 49 (2013) 210–215.

[39] J. Zhang, B. P. Ting, N.R. Jana, Ultrasensitive electrochemical DNA biosensors based on the detection of a highly characteristic solid-state process, Small 5 (2009) 1414–1417.

[40] J.A. Hansen, R. Mukhopadhyay, J. Hansen, K.V. Gothelf, Femtomolar electrochemical detection of DNA targets using metal sulfide nanoparticles, J. Am. Chem. Soc. 128 (2006) 3860–3861.

[41] J. Wang, G.D. Liu, A. Merkoçi, Electrochemical coding technology for simultaneous detection of multiple DNA targets, J. Am. Chem. Soc. 125 (2003) 3214–3215.

[42] F.Y. Kong, B.Y. Xu, J.J. Xu, H.Y. Chen, Simultaneous electrochemical immunoassay using CdS/DNA and PbS/DNA nanochains as labels, Biosens. Bioelectron. 39 (2013) 177–182.

[43] B.J. Cai, S.T. Wang, L. Huang, Y. Ning, Z.Y. Zhang, G.J. Zhang, Ultrasensitive label-free detection of PNA-DNA hybridization by reduced graphene oxide field-effect transistor biosensor, ACS Nano 8 (2014) 2632–2638.

[44] B. Alessandra, P. Martin, Graphene platform for hairpin-DNA-based impedimetric genosensing, ACS Nano 5 (2011) 2356–2361.

[45] J. Lou, S.S. Liu, W.W. Tu, Z.H. Dai, Graphene quantums dots combined with endonuclease cleavage and bidentate chelation for highly sensitive electrochemiluminescent DNA biosensing, Anal. Chem. 87 (2015) 1145−1151.

[46] Q.C. Zhao, Y.Y. Zhou, Y.Y. Li, W. Gu, Q. Zhang, J. Liu, Luminescent iridium(III) complex labeled DNA for graphene oxide based biosensors, Anal. Chem. 88 (2016) 1892–1899.

[47] T.W. Lin, H.Y. Wu, T.T. Tasi, Y.H. Lai, H.H. Shen, Surface-enhanced Raman spectroscopy for DNA detection by the self-assembly of Ag nanoparticles onto Ag nanoparticle-graphene oxide nanocomposites, Phys. Chem. Chem. Phys. 17 (2015) 18443–18448.

[48] J.L. Ma, B.C. Yin, H.N. Le, B.C. Ye, Label-free detection of sequence-specific DNA based on fluorescent silver nanoclusters-assisted surface plasmon-enhanced energy transfer,

ACS Appl. Mater. Interfaces 7 (2015) 12856−12863.

[49] K.J. Huang, Y.J. Liu, H.B. Wang, Y.Y. Wang, A sensitive electrochemical DNA biosensor based on silver nanoparticles-polydopamine@graphene composite, Electrochim. Acta 118 (2014) 130–137.

Scheme and Figure Captions

Fig. 1 Schematic diagram for fabrication process hybridization application of the AgNPs-based DNA biosensor.

Fig. 2 SEM images of S1/AuE (A), GONs/S1-MCH/AuE before (B) and after incubation in HQ/Ag(I) mixture (C) or HQ (E). (D) and (F) are respectively the high-resolution SEM image and EDS analysis result of GONs/S1-MCH/AuE after incubation in HQ-Ag(I) mixture.

Fig. 3 CVs (A) and Nyquist plots (B) of (a) bare AuE, (b) S1/AuE, (c) S1-MCH/AuE and (d) GONs/S1-MCH/AuE in 1mM $[Fe(CN)_6]^{3-/4-}$ and 0.1 M KCl mixture. The scan rate for CV tests is 100 mV s^{-1}. EIS were collected in the frequency range from 0.01 Hz to 10^4 Hz, at an applied potential fo +0.200 V.

Fig. 4 (A) CVs of GONs/S1-MCH/AuE (a), AgNPs/S1-MCH/AuE (b), and AgNPs/GONs/S1-MCH/AuE (c) in the supporting electrolyte of 0.1 M KCl. The scan rate is 100 mV s^{-1}. (B) Dependence of CVs of AgNPs/GONs/S1-MCH/AuE on scan rate (v) in 0.1M KCl solution (B). Inset is the relationship of I_p with $v^{1/2}$.

Fig. 5 CVs of AgNPs/GONs/S1-MCH/AuE (A) and AgNPs/S1-MCH/AuE (B) before (a) and after (b) hybridization with 0.1 pM complementary DNA (S2). The other conditions are the same with Fig. 4A.

Fig. 6 (A) Effect of GONs incubation time (t) on charge transfer resistance (R_{ct}) in EIS measurements. (B) Effect of DNA hybridization time (t) on the DPV peak currents (I_{pa}).

Fig. 7 (A) DPVs of AgNPs/GO/S1-MCH/AuE upon hybridization with 0 M (a), 10.0 fM (b), 0.1 pM (c), 1.0 pM (d), 10.0 pM (e), 0.1 nM (f), 1.0 nM (g) 10 nM (h) target DNA of S2. (B) Linear relationship of oxidation peak current (I_{pa}) versus the logarithm values of S2

concentration ($\lg C_{S2}$).

Fig. 8 (A) DPVs of AgNPs/GONs/MCH-S1/AuE before (a) and after hybridization with complementary sequence of S2 (b), one-base mismatched sequence of S3 (c), three-base mismatched sequence of S4 (d), and non-complementary sequence of S5 (e). All the concentrations of hybridized sequences are 1.0×10^{-13} M. (B) Bar chart of the oxidation peak current (I_{pa}) obtained for different hybridized electrodes.

Table titles

Table 1 Comparison of analytical performance of DNA biosensors based on AgNPs or graphene materials.

Table 2 Recovery test of target DNA in serum samples by the biosensor

Scheme and Figures

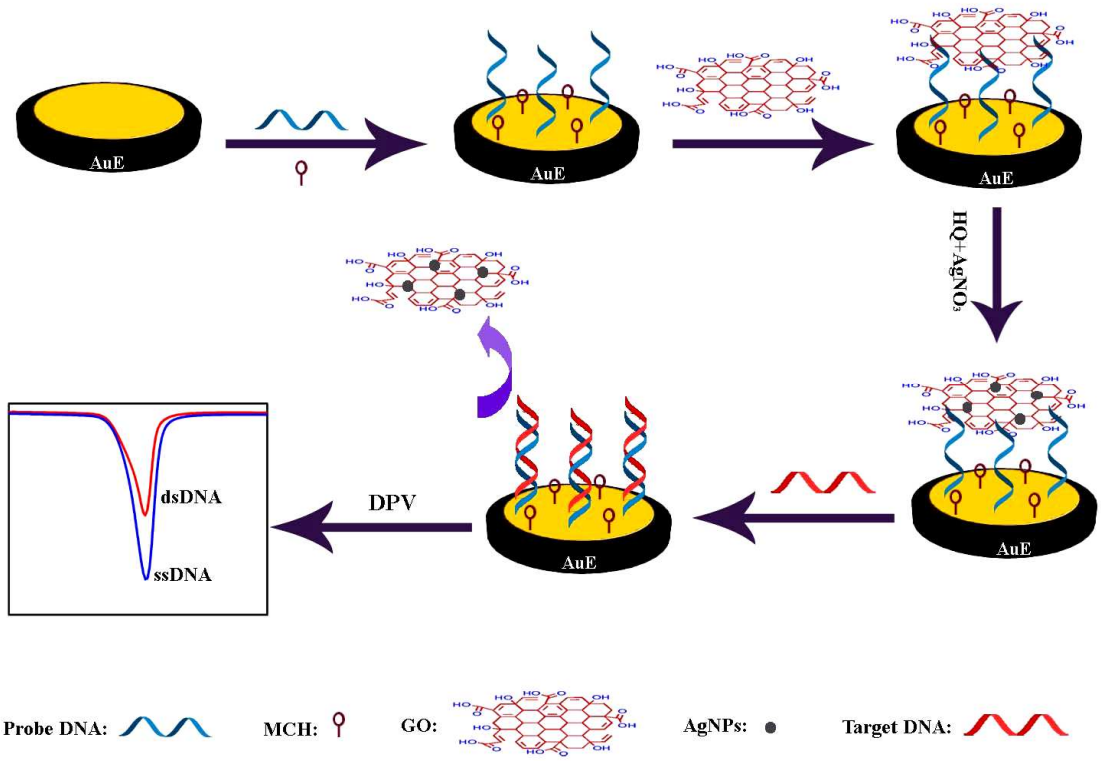

Fig. 1

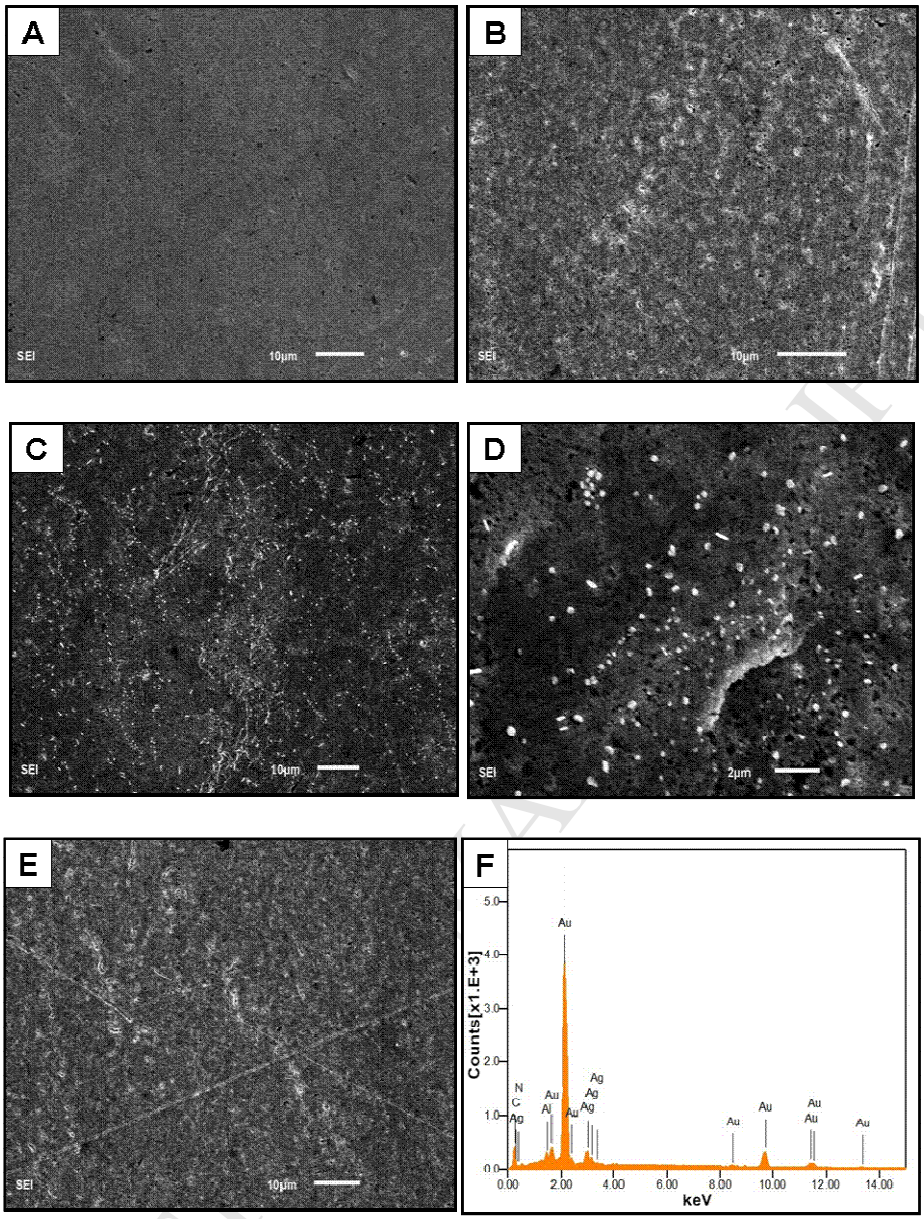
A
SEI
10µm
B
SEI
10µm
C
SEI
10µm
D
SEI
2µm
E
SEI
10µm
F
Counts[x1.E+3]
5.0
4.0
3.0
2.0
1.0
0.0
N
C
Ag
Au
Al
Au
Au
Ag
Ag
Ag
Au
Au
Au
Au
Au
0.00
2.00
4.00
6.00
8.00
10.00
12.00
14.00
keV

Fig. 2

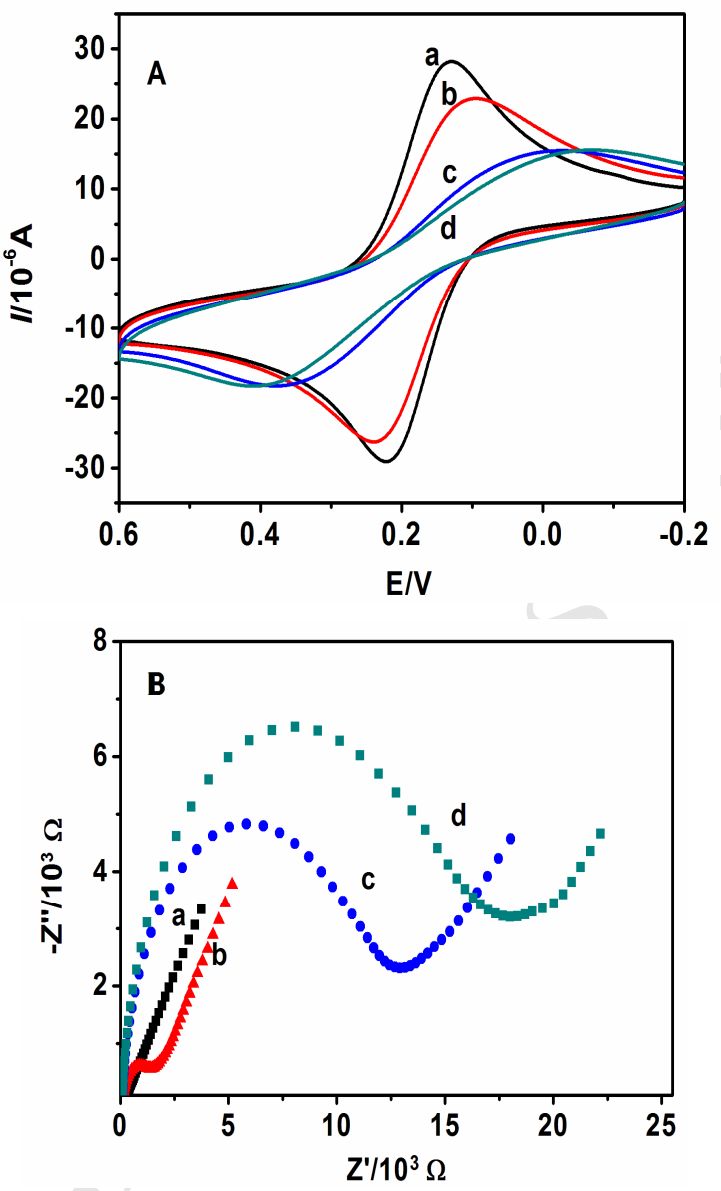
A
a
b
c
d
I/10^-6 A
E/V
30
20
10
0
-10
-20
-30
0.6
0.4
0.2
0.0
-0.2
B
-Z''/10^3 Ω
Z'/10^3 Ω
8
6
4
2
0
5
10
15
20
25

Fig. 3

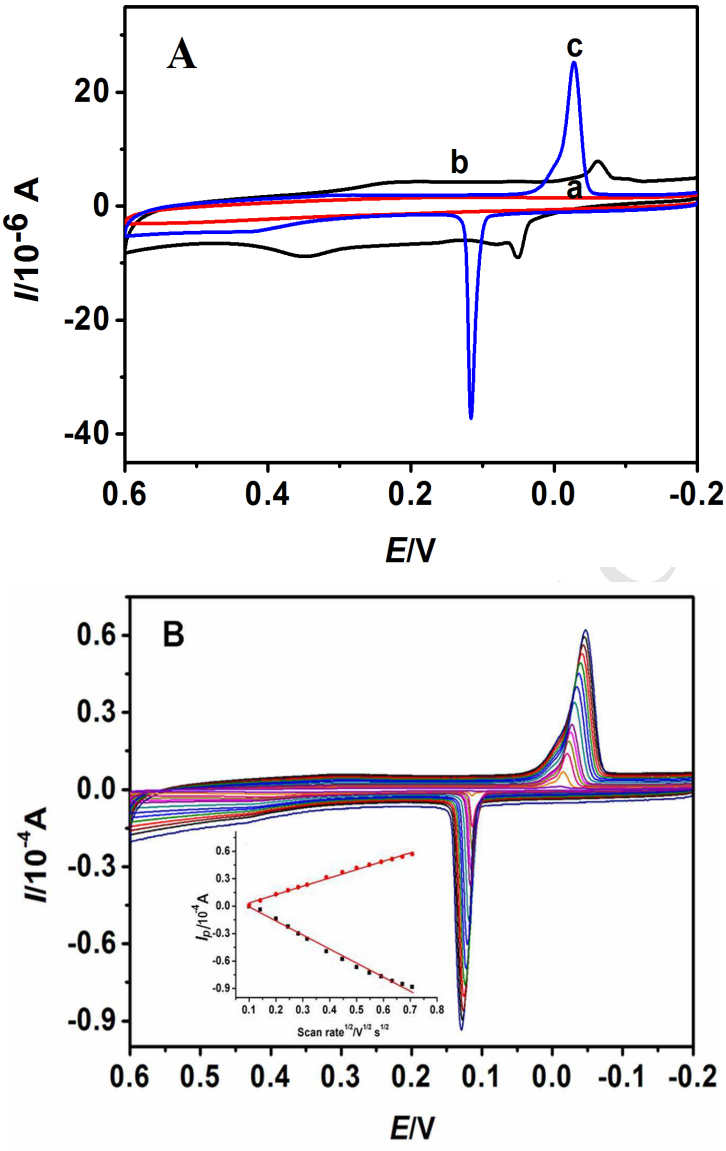
A
c
b
a
20
0
-20
-40
I/10-6 A
0.6
0.4
0.2
0.0
-0.2
E/V
B
0.6
0.3
0.0
-0.3
-0.6
-0.9
I/10-4 A
0.6 0.5 0.4 0.3 0.2 0.1 0.0 -0.1 -0.2
E/V
Ip/10-4 A
Scan rate1/2/V1/2 s1/2

Fig. 4

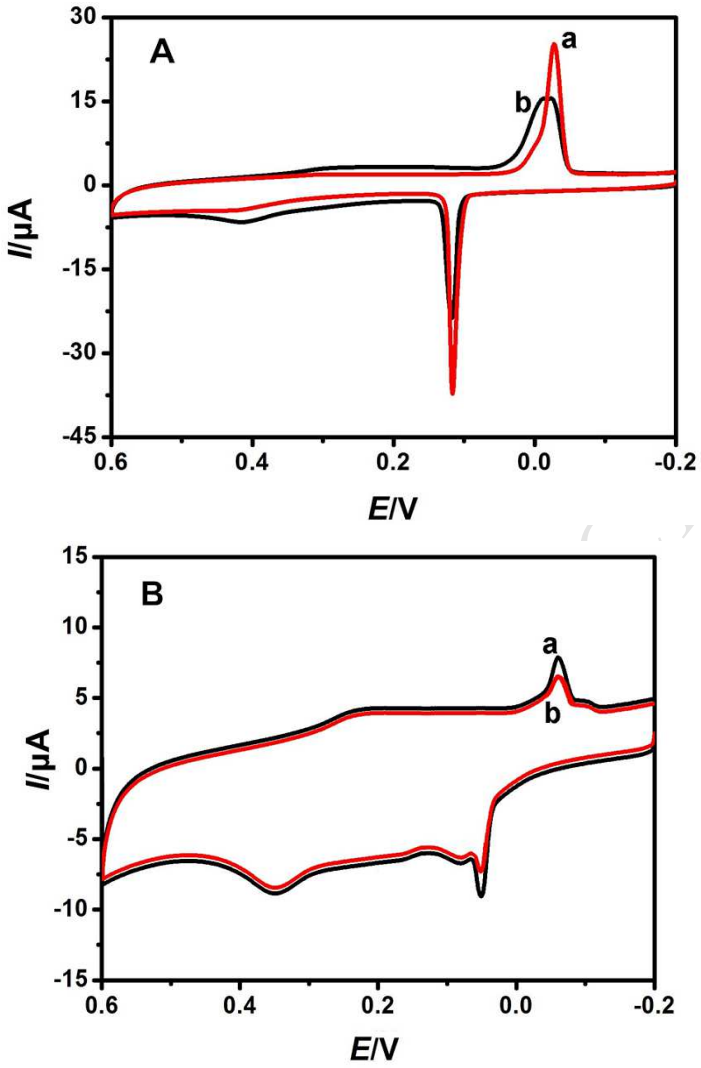

Fig. 5

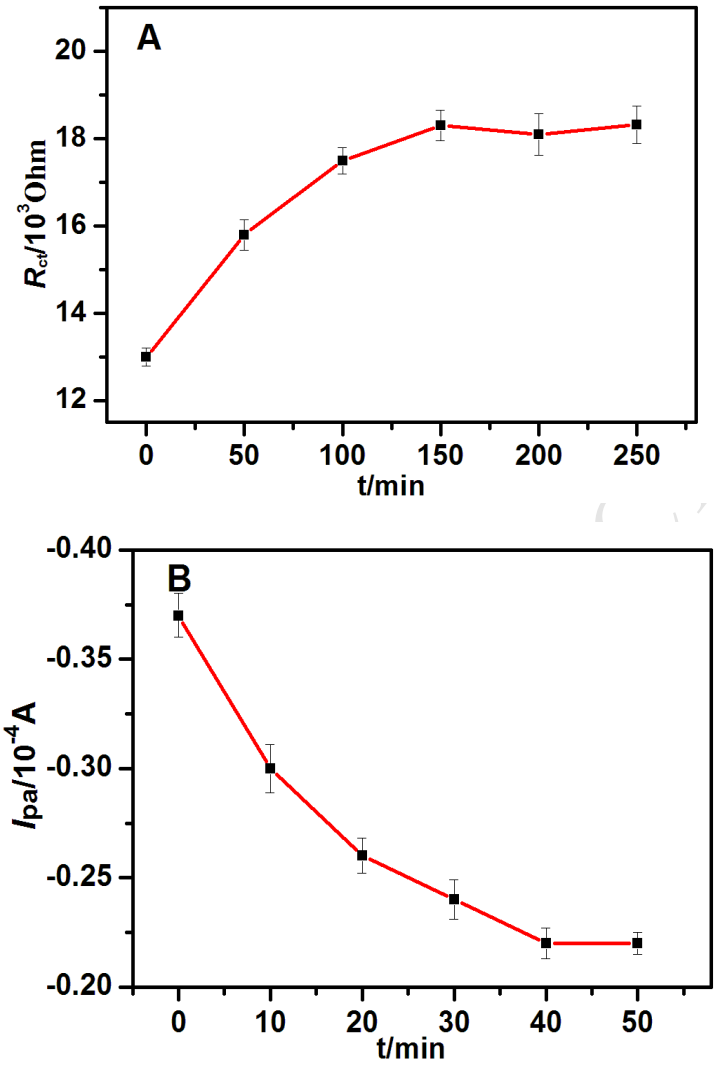
A
20
18
16
14
12
$R_{ct}/10^3$Ohm
0
50
100
150
200
250
t/min
B
-0.40
-0.35
-0.30
-0.25
-0.20
$I_{pa}/10^{-4}$A
0
10
20
30
40
50
t/min

Fig. 6

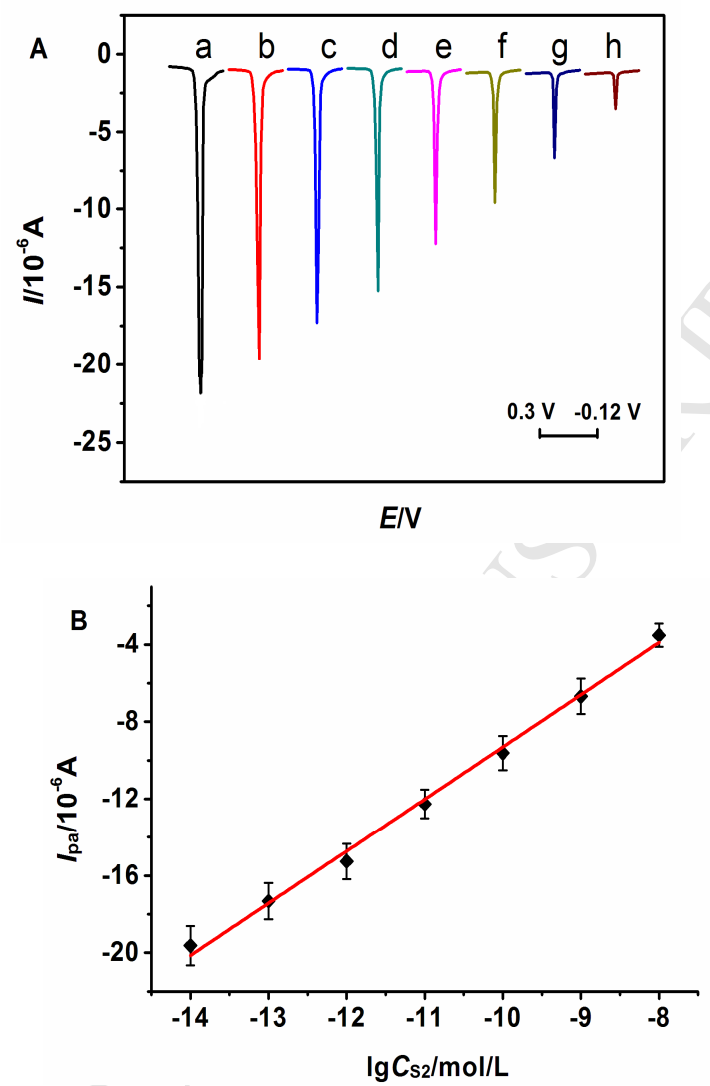
A
a
b
c
d
e
f
g
h
0
-5
-10
-15
-20
-25
I/10-6A
0.3 V
-0.12 V
E/V
B
-4
-8
-12
-16
-20
Ipa/10-6A
-14
-13
-12
-11
-10
-9
-8
lgCS2/mol/L

Fig. 7

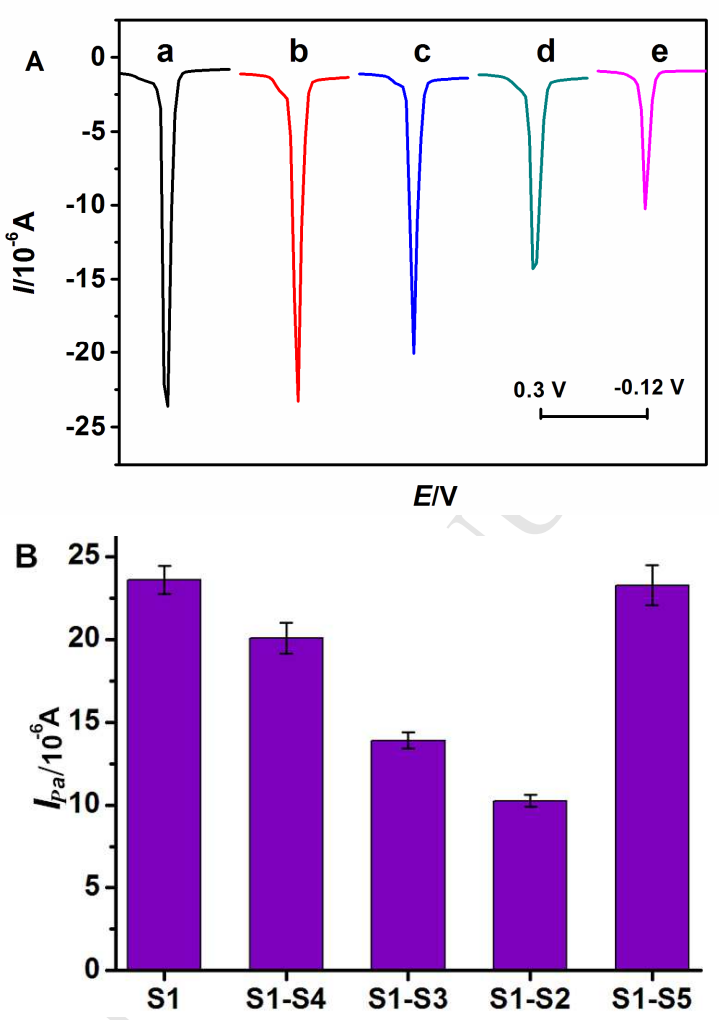
A
a
b
c
d
e
0
-5
-10
-15
-20
-25
I/10^-6 A
0.3 V
-0.12 V
E/V
B
25
20
15
10
5
0
I_pa/10^-6 A
S1
S1-S4
S1-S3
S1-S2
S1-S5

Fig. 8

Table 1 Comparison of analytical performance of DNA biosensors based on AgNPs or graphene materials.

Sensing platforms	Methods	Linear ranges	Detection limits	Refs.
RGO	FET	10 f M-1.0 nM	100 fM	[43]
G-FL	EIS	-	6.6 pM	[44]
GQDs	ECL	5.0 fM-10.0 nM	0.45 fM	[45]
GO	Fluorescence	5.0 nM-50.0 nM	-	[46]
AgNPs	SERS	1.0 pM -1.0 nM	1.0 pM	[47]
AgNCs	SPEET	5 nM-100 nM	2.5 nM	[48]
AgNPs-Pdop@GR	EC	0.1 pM -10.0 nM	3.2 nM	[49]
AgNPs/GONs	EC	10 fM-10 nM	7.6 fM	This Work

Notes: RGO: Reduced graphene oxide; FET: Field-effect transistor; G-FL: four layer graphenes; GQDs: Graphene quantum dots; ECL: Electrochemiluminescence; SERS: Surface-enhanced Raman spectroscopy; SPEET: Surface plasmon enhanced energy transfer; AgNPs-Pdop@GR: AgNPs-polydopamine@graphene; EC: Electrochemistry.

Table 2 Recovery test of target DNA in serum samples by the biosensor

Serum samples	Added	Found	Recovery (%)	RSD (%)
1	0.100 nM	0.107 nM	107.0	3.98
2	1.00 pM	0.96 pM	96.0	4.36
3	10.0 fM	9.52 fM	95.2	5.67

Highlights

- An novel DNA biosensor was constructed based on GONs with deposited AgNPs
- GONs catalyze the in-situ deposition of AgNPs on the sensing interface
- Unique π-stacking of GONs with probe DNA contributes high selectivity of the biosensor
- High electroactivity of AgNPs leads to low detection limit (7.6 fM) for target DNA